Chapter 4

Iron-Iron carbide (Fe/Fe_3C) Encapsulated in S, N Co-doped Graphitic Carbon as Robust HER Electrocatalyst

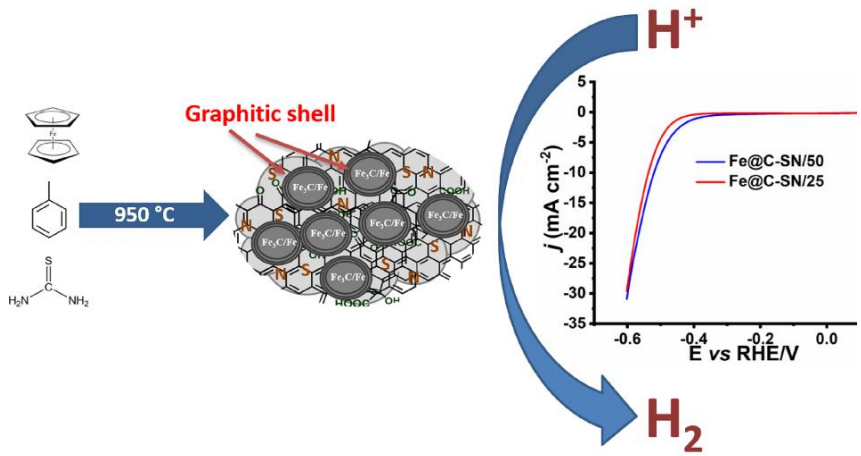

This chapter is a contribution to the quest of noble metal-free HER electrocatalyst, where transition metal-based carbide encapsulated into doped carbon matrix was prepared using a low-cost, one-step pyrolytic method. The as-prepared nanomaterials were investigated for catalytic hydrogen evolution reaction (HER) in an acidic medium.

4.1 Introduction

With the depletion of fossil-based fuels and challenges like climate change, dependence and demand for clean energy are pacing up. [110,112] It has directed the current research effort for the development of materials possessing high efficiency for energy conversion and energy storage. In the USA, renewables have become the second-most prevalent electricity source (21%) in 2020, as per the recent report. [152] Energy from hydrogen carrier has proved to be efficient and cleaner and its commercial production has already begun. Hydrogen fuel is a zero-emission fuel that burns with oxygen, leaving no harmful side products. Hydrogen generation and hydrogen storage both are economically upfront for many countries. [153-155] Water has served the purpose of hydrogen fuel generation by the phenomenon of water splitting at a thermodynamic potential of 1.23 V under ideal conditions. At the experimental stage, catalysts having certain overpotential values are always required to speed up the sluggish reaction. [60,156] Platinum and some other noble metals like Rh, Ir (and their oxides) are categorized as good water-splitting catalysts, but high cost and low availability have restricted their commercial use. The quest to find an alternative has led to the exploration of many earth-abundant elements and non-noble metal-based electrocatalysts such as graphitic carbon nitride (g-C_3N_4) based HER catalysts, [122,157] transition metal dichalcogenides (TMDCs) like MoS_2, WS_2, WSe_2, [115,116,119,151,158] nitrides, carbides and carbon-based catalyst are few examples in this advent of non-noble earth-abundant electrocatalysts. [159]

Transition metal carbides have attracted great interest in the past few years owing to their competitive catalytic behavior to that of Pt-based catalysts. [160] Iron carbide, in this regard, has come out as a prominent candidate since it forms

composites with carbon materials (CNT, graphene, meso/macroporous carbon) and their synergistic effects have shown enhanced catalytic performance. [161-164] Earlier synthesis reports on iron carbide involve a multi-step synthesis process from various precursors and templates. [161, 163-167] Graphitic carbon encapsulated iron carbide has been explored for its excellent magnetic properties, but the quest for low-cost synthetic routes with excellent electrochemical properties (especially HER and ORR) is still on. [162-164] Doping with heteroatoms such as N/S/O alters the electronic structure and enhances the number of sites where H^+ can adsorb prior to reduction. The presence of heteroatoms (N) in carbon encapsulation has always exhibited an increase in the activity of graphite encapsulated iron carbide species. [161,162,166] Sulphur as metal sulfides (as MoS_2) has shown promising HER activity close to platinum when prepared in edge-on orientation. [116,119,158] Both the elements S and N are appropriate choices for enhancement in catalytic properties when present in the carbon matrix.

In this work, we report a low-cost, one-step pyrolytic method to synthesize carbon encapsulated iron carbide species, similar to earlier reports. [168-170] In view of available reports about carbon encapsulated iron carbide species, we, in our research study, prepared dual heteroatom-doped carbon encapsulated nanoscale iron/iron carbide species in a one-step synthesis process. Cheap precursors, like ferrocene and toluene, were used as base materials, while heteroatom doping was achieved by varying different weights of thiourea. The dopant species N obtained from thiourea gets incorporated in graphitic carbon encapsulation as pyridinic/pyrrolic/graphitic N form while S majorly as thiophene form, which are well confirmed from high-resolution XPS spectra. [171,172] Incorporation of these heteroatoms creates several active sites, which significantly alter the catalytic

performance. Hydrogen ion (H^+) has a great affinity to get adsorbed on these heterospecies, where it gets further reduced into H_2. We observed that there is an optimum critical amount of thiourea (20 wt. %) that gives the optimum S, N- active sites on the carbonaceous surface, which led to significant enhancement in hydrogen evolution reaction (HER) with lowest onset to start the evolution process among all species. Sample prepared from 10% thio urea addition also excels in HER activity (lowest Tafel slope) and shows maximum double layer capacitance value (C_{dl}) among other variants. The onset potential of HER is lowest for sample with 20% addition of thiourea. The complete structural and morphological analysis of doped variants of carbon encapsulated iron/iron carbide species have been done along with elemental analysis by XPS technique and surface area measurements in the following sections. It was followed by measurements of electrocatalytic HER activity in acidic medium with details of increase in performance ending in concluding remarks.

4.2 Experimental Section

4.2.1 Materials

Ferrocene ~ 98% (Dicyclopentadienyliron) was obtained from Spetrochem, while toluene ~ 99.5% purity (GC) and thiourea (≥99.0%) were purchased from Merck. All chemicals were used as received without further purification.

4.2.2 Synthesis of S, N co-doped iron/iron carbide

For the synthesis of heteroatom doped carbon encapsulated iron/iron carbide, we took a 45 cm long one side sealed quartz tube (diameter 1.0 cm) and added 250 mg of ferrocene, 2 ml of toluene and 50 mg of thiourea, and sonicated for 10 minutes to mix it properly. We kept small quartz pieces to the open side of the tube as an

obstruction and fitted a thick-walled N_2 filled latex balloon to separate the reaction mixture from the outer environment. Quartz tube with the closed-end having mixture was kept in a slightly tilted position along the tubular furnace, while the open end remained outside. Glass wool was used to close the opening of the furnace properly to prevent any heat loss. The furnace was programmed with a reaction temperature of 950 °C for 10 h and ramping rate of 3°C/minute. After cooling the furnace naturally, the sample was collected by scratching and washed with dichloromethane multiple times to remove any unreacted precursors and organic impurities. The collected sample was labeled as Fe@C-SN/50 and dried at 80 °C in a vacuum oven overnight. Figure 4.1 depicts the graphical synthesis protocol we followed. Similar method was adopted for the synthesis of 25 mg (10%) and 75 mg (30%) thiourea added iron carbide species and labeled as Fe@C-SN/25 and Fe@C-SN/75, respectively. For the synthesis of the undoped variant, labeled as Fe@C, the same protocol was followed in the absence of thiourea.

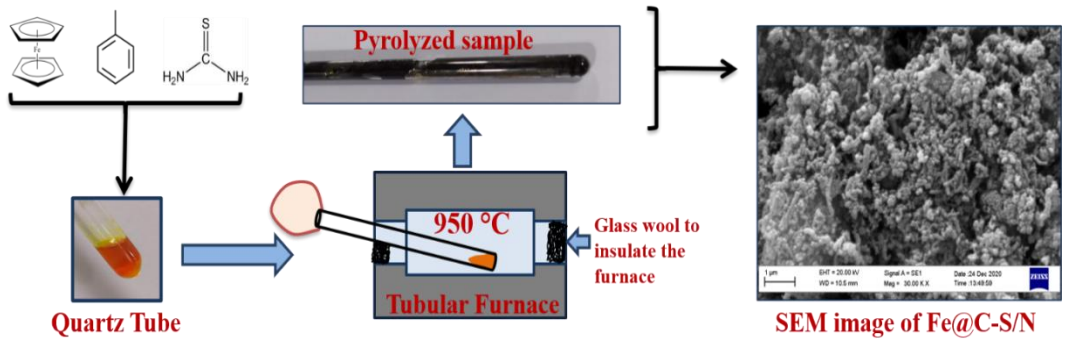

Fig. 4.1 Synthesis protocol of doped carbon encapsulated iron-iron carbide (Fe/Fe_3C).

4.2.3 Instrumentations

XRD data were obtained from Rigaku MiniFlex BENCHTOP 600 W X-ray diffractometer having Ni-filtered Cu $K_{\alpha 1}$ radiation (λ=1.54056 Å) at a scan rate of 3°min^{-1}. X-ray photoelectron spectrum (XPS) was obtained from the Thermo Fischer Scientific K-alpha XPS system, the energy of the source is Al K_{α} energy line of X-ray with 1487.6 eV of energy. Raman data was collected using an STR-300 spectrometer with a green laser of excitation wavelength 532 nm. SEM images and EDAX were collected from Carl Zeiss, model Supra 40. Transmission electron microscope (TEM) images were acquired from FEI, TECHNAI G^2 20 TWIN instrument at accelerating voltage of 200 kV. Surface area measurement and pore size distribution analysis were carried out in the BELLSORP MAX II model of Microtrac BEL Corp. using N_2 gas at liquid N_2 temperature of 77K.

4.3 Results and Discussion

4.3.1 Structural and morphological Study of as-prepared samples

The prepared sample was first characterized using the XRD technique to confirm the synthesis of desired materials. XRD spectra (Fig. 4.2 (a)) of all the samples exhibit a major peak at 2θ = 26.4° followed by a series of small peaks in 35 to 55° of 2θ range. The peak at 26.4° is designated to the graphitic phase of carbon (inorganic crystal structure data; ICSD code-76767), which belongs to (002) reflection plane. As we increased the amount of thiourea from 25 to 75 mg in precursor mixture, an increase of relative peak intensity was observed, indicating increasing graphitic phase of carbon in the prepared sample Fe@C-SN/25, Fe@C-SN/50 and Fe@C-SN/75. It reveals the role of thiourea in graphitization besides providing dopant elements Sulphur and nitrogen. Various small peaks present in 2θ

range of 35 to 55° belong to Fe-based crystalline phases viz. Fe_3C (major), α-Fe (bcc), γ-Fe (fcc), and graphite. Figure 4.2 (b) represents these phases in detail along with diffraction planes, peak at 2θ = 45.0° confirms the presence of α-Fe (ICSD code-44863), while peaks at 2θ = 43.8° and 50.9° confirms γ-Fe (ICSD code-44862) phase. Major diffraction peaks at 35.8°, 37.9°, 39.9°, 40.8°, 43.0° and 45.9° belong to the crystalline Fe_3C (ICSD code- 99002) phase. Graphitic carbon peak is present at 2θ = 48.9° (ICSD code-16593). Compared to the undoped sample, the doped samples contain more crystalline phases. A small amount of Fe_3O_4 phase was also observed at 2θ = 35.5° owing to the presence of trace oxygen in the synthesis tube.

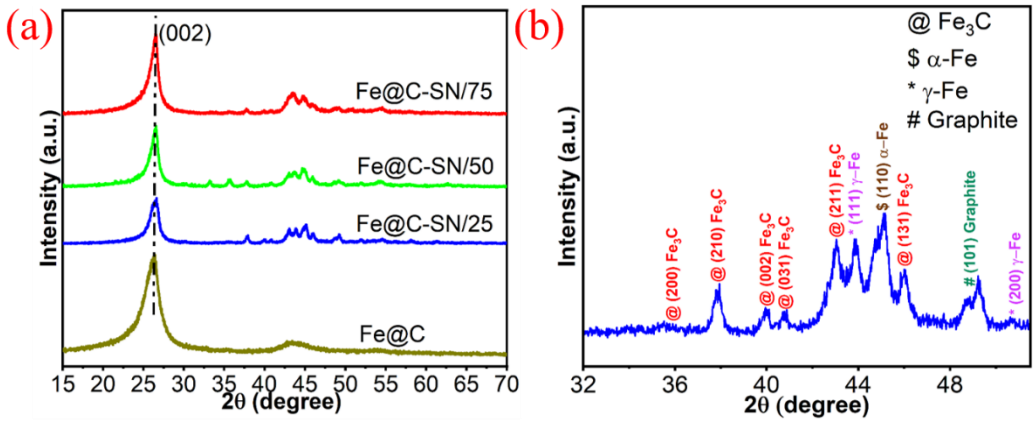

Fig. 4.2 (a) XRD spectra of iron carbide and its doped variants and (b) Zoomed-in XRD pattern of Fe@C-SN/25 from 2θ = 35 to 55° range.

After confirmation of crystallographic phases in the doped species of carbon encapsulated iron carbide by XRD patterns, morphological study of the as-prepared samples was done by Electron microscopy (SEM and TEM-HRTEM). Figure 4.3 shows the SEM images acquired at the magnification scale of 1μm of Fe@C and other doped species of Fe@C viz. Fe@C-SN/25, Fe@C-SN/50 and Fe@C-SN/75. The bottom-up synthesis approach yields aggregated (globular type) morphology

for all the prepared samples. Tubular structures are also visible which are synthesized at lesser heated parts of the tube. Such morphology can be easily justified from the earlier reported papers of Kumar et al. [168] The growth mechanism of such nanostructures has been published elsewhere. [168, 173, 174] Briefly, in this route, the organometallic precursor and carbon source are taken in closed-end quartz tubes and subjected to pyrolysis in a tube furnace. These precursors vaporize and reach the central high-temperature zone along the pressure gradient, where they decompose and form nuclei. These nuclei may be in metal oxide form, which gets reduced in the presence of the carbonaceous environment during pyrolysis. Since iron has relatively low metallicity, [175] it prefers to form iron carbide rather than

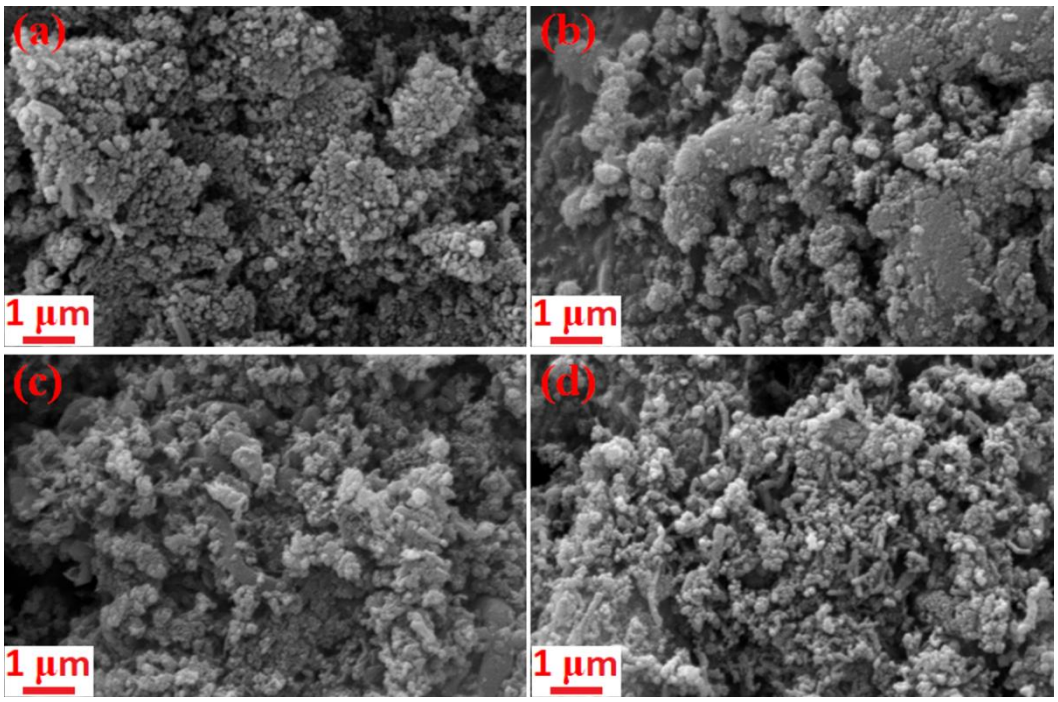

Fig. 4.3 SEM images of (a) Fe@C, (b) Fe@C-SN/25, (c) Fe@C-SN/50 and (d) Fe@C-SN/75.

iron metal. The iron/iron carbide formed acts as a catalyst for the growth of carbon nanostructures, which predominantly follows the vapor-liquid-solid (VLS) mechanism. [173] Doping of S- and N- in graphitic encapsulation does not affect the overall morphology as all doped samples exhibits similar texture as of Fe@C.

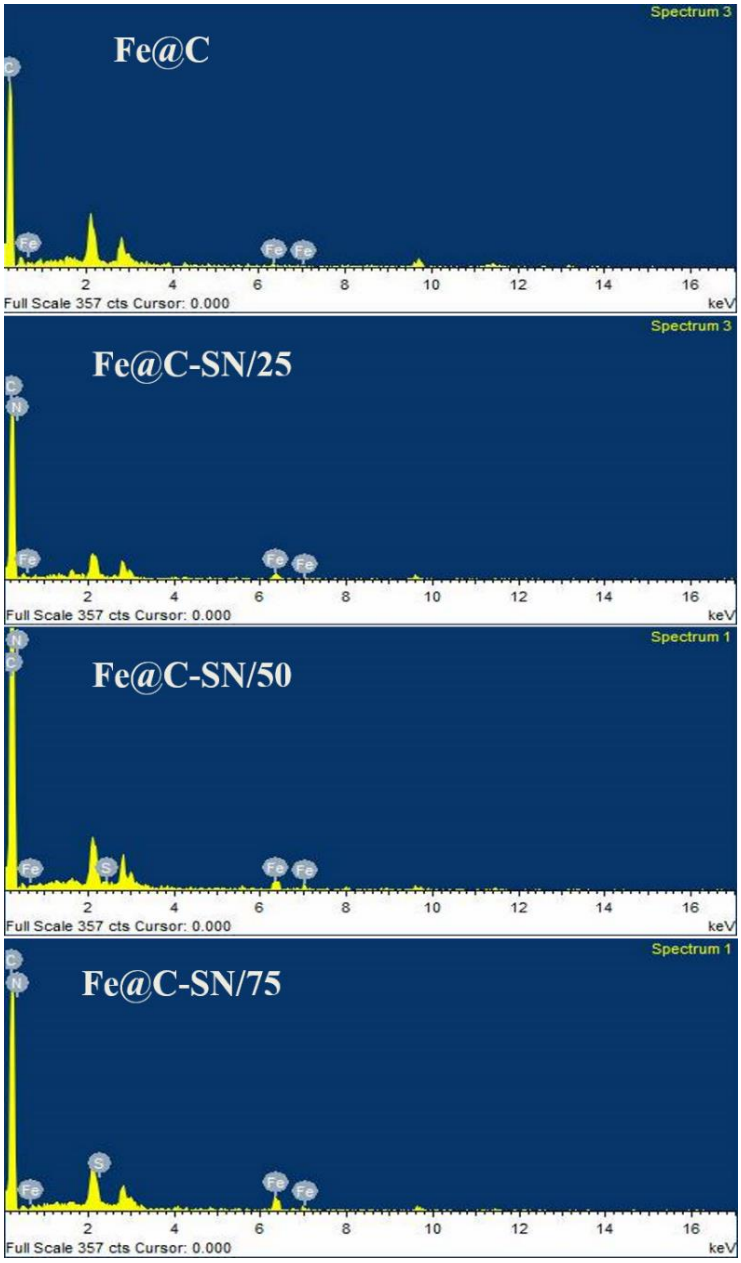

Fig. 4.4 SEM EDX spectra of the as-prepared samples.

Prepared samples are porous and sizes of globules are limited to few hundred nanometers in all the specimens. The EDX spectra (*see* Fig. 4.4) of the corresponding samples confirm the presence of all the elements supposed.

Transmission electron microscopic images (Fig. 4.5 a) further justified the core-shell nature of the prepared samples. Fe/Fe_3C makes core structure with encapsulation of doped graphitic phase of carbon. The HRTEM image shown in Figure 4.5 (b) clearly distinguishes the core structure into the carbon matrix. The d-spacing of the graphitic shell was found to be 0.336 nm, while for the iron carbide part, it is 0.182 nm. SAED pattern (Fig. 4.5 c) has concentric circles along with bright spots which verify the crystalline nature of Fe/Fe_3C core along with amorphous carbon matrix.

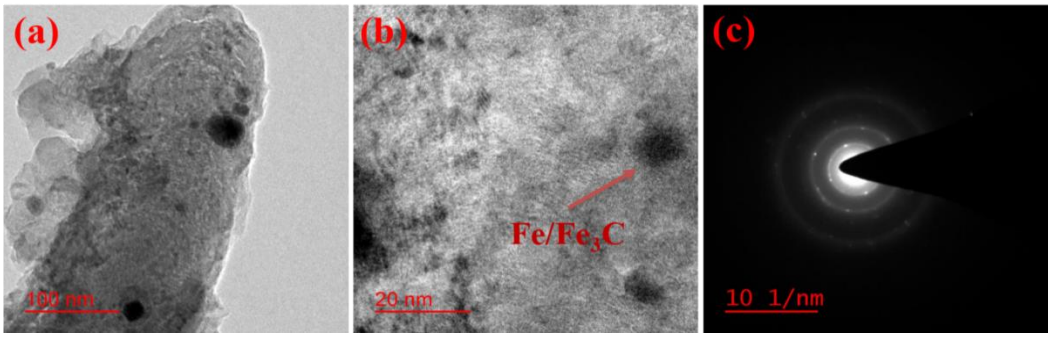

Fig. 4.5 TEM and HRTEM images of Fe@C-SN/50 along with SAED pattern.

4.3.2 Elemental Analysis

After structural and morphological analysis, X-ray photoelectron spectroscopy (XPS) was performed to confirm the elemental state along with dopant species. The full scan survey spectrum contains peaks of Fe, C, S and N along with the peaks of

O owing to atmospheric oxygen (*see* Appendix A Fig. A.5). Figure 4.6 exhibits the deconvoluted peaks of constituting elements of all doped variants of Fe@C, the high-resolution peaks of Fe and C of undoped Fe@C is included in Appendix A Figure A.6. The intensity of the Fe peak is significantly lower than its surrounding carbon as it makes the core part of the sample. It can be noted that the penetration depth of Ar+ ions in the XPS technique is ~ 10 nm. The high-resolution Fe2p peak (Fig. 4.6 (A, B and C)) has the presence of the metallic Fe (0) at ~707 eV, while other oxidation states of Fe (+2 and +3) also appear, including satellite peaks. The high-resolution C1s spectrum has been deconvoluted into six peaks attributed to various bonding states of C viz. C-Fe, C=C, C-C, C-O/C-N/C-S, C=O and O-C=O. [170] Doped N1s has five deconvolution peaks attributed to pyridinic, amino, pyrrolic, graphitic and oxidized N as seen in Figure 4.6 (G, H and I). S2p deconvoluted spectrum has peaks corresponding to bonding state C-S-C, C-S-H, thiophene, $-SO_3H$ and oxidized S. [92]

The binding energies corresponding to various chemical environments of elements present are also tabulated in Appendix A Table A.2. Deconvolution of elemental species shows that S and N have now become an integral part of carbon shell-matrix and are exposed as active sites where H+ has a greater affinity to adsorb resulting in faster H_2 evolution in doped species. The atomic % of the elements present at the surface of the samples is also shown in Table 4.1. The % content of Fe is low and is attributed to its being a core component since the low penetration depth of Ar+ ions.

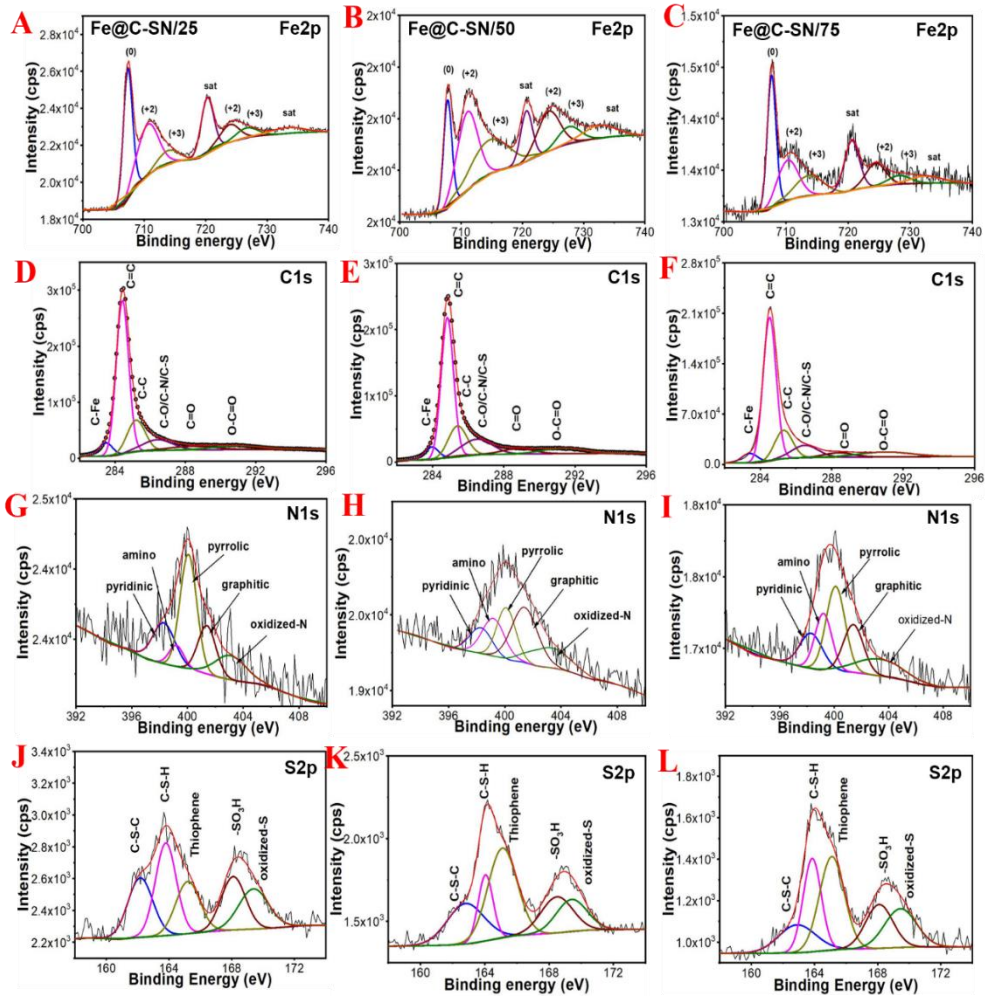

Fig. 4.6 High resolution deconvoluted Fe2p, C1s, N1s and S2p peaks of doped Fe@C-SN/25, Fe@C-SN/50 and Fe@C-SN/75 samples.

Table 4.1 Atomic % of elements present at the surface of the samples analyzed from XPS analysis

	Fe (at%)	C (at%)	S (at%)	N (at%)
Fe@C	0.32	99.68	-	-
Fe@C-SN/25	0.91	98.61	0.18	0.30
Fe@C-SN/50	0.25	98.61	0.76	0.38
Fe@C-SN/75	0.04	98.96	0.43	0.57

.

4.3.3 Raman Study and Surface Area Analysis

In order to get critical insights into the catalytic performance of the samples, the role of defects was envisaged through Raman spectroscopy. Figure 4.7 exhibits the deconvoluted D and G band characteristics of the disorder and graphitic phase of carbon of doped and undoped Fe@C species. Each spectrum was fit with four D-peaks and one G-peak. [176-178] D1 peak belongs to C=C in-plane vibration, D2 to graphitic crystallite edges, D3 to amorphous carbon and last D4 peak belongs to sp^2-sp^3 bond or C-C/C=C stretching mode in the conjugated system. The high intensity of the D1 peak signifies micro crystallinity and distortion of graphitic carbon. The ratio of I_G/I_D, which is used to quantify the level of the defect in the prepared samples was found to be 0.33, 0.39, 0.20 and 0.34 for Fe@C, Fe@C-SN/25, Fe@C-SN/50 and Fe@C-SN/75 samples, respectively, suggesting greater defects in the doped samples. Appendix Table A.3 contains peak position of various peaks obtained along with their area and FWHM

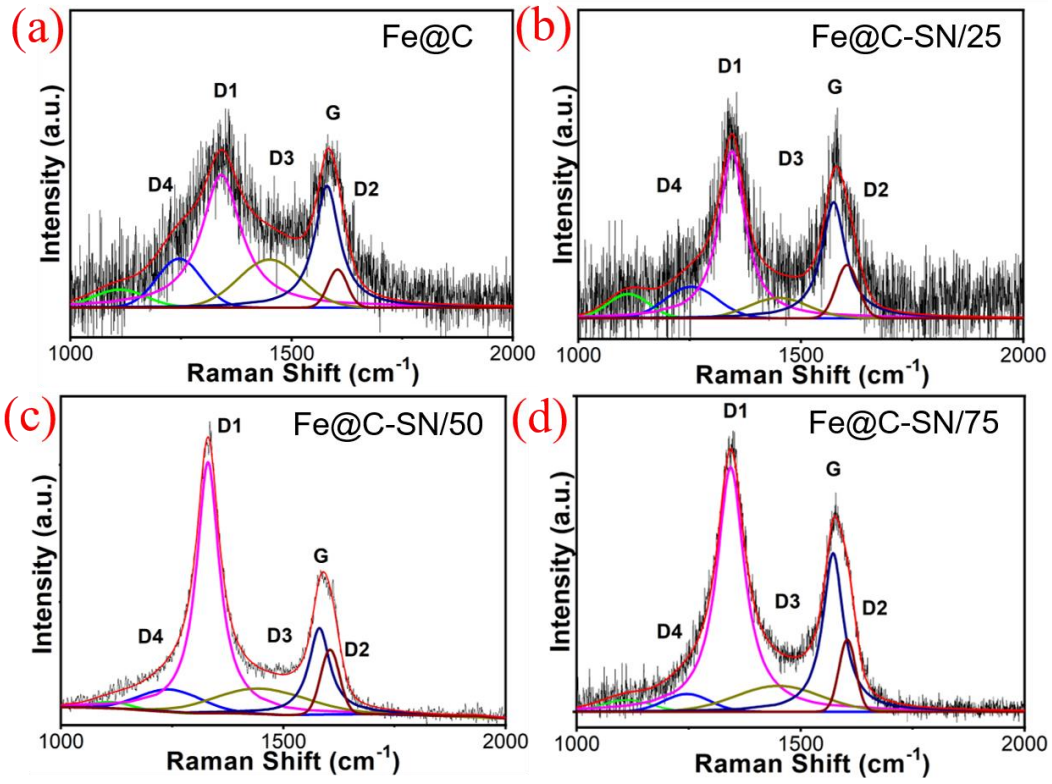

Fig. 4.7 Raman spectrum of the synthesized samples.

Since water electrocatalysis is a surface-based phenomenon where H^+ is adsorbed over specific sites and gets reduced into H_2 by cathodic electron, determination of the surface area of the catalyst is another important measurement to reveal its micro/mesoporous nature and pore size information. The surface area was determined from the BET (Brunauer–Emmett–Teller) plot using N_2 adsorption-desorption isotherm at liquid N_2 temperature of 77 K. We took the good HER performing samples (Fe@C-SN/25 and Fe@C-SN/50). Figure 4.8 displays the N_2 isotherm of type IV along with pore volume distribution in the inset plot. The specific surface area obtained from the single-point BET plot is 35.73 and 31.50 m^2g^{-1}, while the average diameter of pore obtained from BJH (Brunauer-Joyner-Halenda) theory is 18.74 and 19.52 nm for Fe@C-SN/25 and Fe@C-SN/50,

respectively. The small surface areas of the samples are because of their intact flaky structure. The pore size confirms the mesoporous nature of samples.

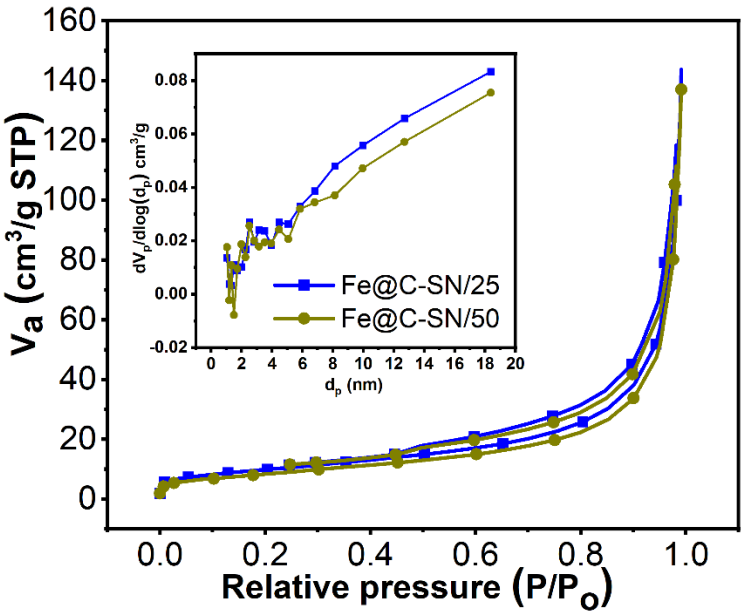

Fig. 4.8 N_2 adsorption-desorption isotherm of equal HER performing catalysts; Fe@C-SN/50 and Fe@C-SN/25. Inset shows pore volume distribution plot of corresponding species.

4.3.4 Electrochemical Measurements

Before measuring the electrochemical catalytic properties of prepared materials, the material's ink was prepared as follows. Typically, 2 mg of the sample was dispersed in 500 µl of water-ethanol (1:1) mixture and 15 µl of Nafion was added as a binder. The dispersion was sonicated for 30 minutes to homogenize the mixture. 10 µl of ink was drop cast (loading amount = 0.554 mg cm^{-2}) over the GC electrode and dried under the tungsten bulb lamp.

All electrochemical measurements were performed in 0.5 M H_2SO_4 on the CHI7044 model electrochemical station having three electrodes set up. Ag/AgCl (in 3M KCl) was chosen as the reference electrode, while platinum wire as the counter electrode. Glassy carbon (GC) electrode having 3 mm diameter acts as working electrode modified with sample's ink. Prior to GC modification, the GC electrode was polished over a polishing pad in 0.05 μ alumina slurry. All the potential values were converted with reference to Reversible Hydrogen Electrode (RHE) as per the following equation

$$E_{RHE} = E_{Ag/AgCl} + 0.059\,pH + E^{0}_{Ag/AgCl} \text{.....(Eq. 4.1)}$$

Figure 4.9 (a) shows the combined HER polarization curves of iron/iron carbide and its various doped variants Fe@C-SN/25, Fe@C-SN/50 and Fe@C-SN/75. All the measurements were performed using an equal amount of catalyst loading of 0.554 mg cm^{-2} over polished GC electrode. The influence of S and N in carbon encapsulation over the catalytic performance of prepared samples is clearly visible as doped species exhibit superior hydrogen evolution performance compared to undoped Fe@C species. The samples with moderate (10 and 20%) thiourea added species, i.e., Fe@C-SN/25 and Fe@C-SN/50 show robust current density with an overpotential value of 537 mV and 520 mV, respectively for 10 mA cm^{-2}. Fe@C-SN/50 requires the least onset potential of 358mV among all the doped species and undoped Fe@C. The hydrogen evolution ability of Fe@C-SN/25 and Fe@C-SN/50 are far better than Fe@C-SN/75. This increase of HER activity is attributed to S and N species present in different bonding states in carbon shell and matrix as confirmed in XPS analysis. Hydrogen has a special affinity for these S and N sites

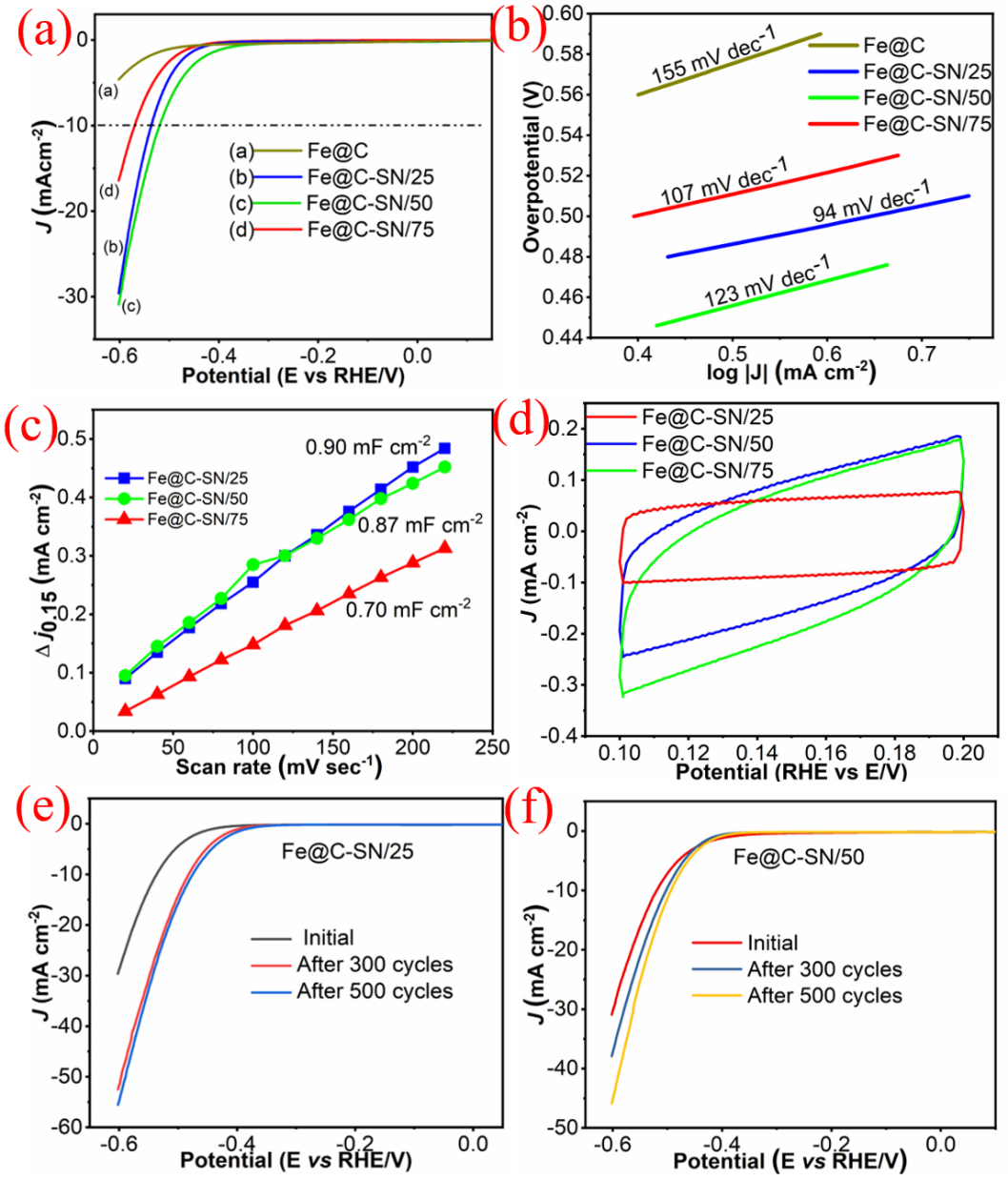

Fig. 4.9 (a) LSV polarization curves (scan rate 5 mV/sec) of Fe@C along with its doped variants; (b) Corresponding Tafel slopes; (c) Calculation of double-layer capacitance (C_{dl}) of doped variants of Fe@C; (d) CVs of doped variants at scan rate of 100 mV sec^{-1}; Stability LSVs of (e) Fe@C-SN/25 and (f) Fe@C-SN/50 after multiple CV sweeps at scans rate of 5 mV/sec.

to get adsorbed, where further reduction into H_2 occurs and can be correlated to cathodic current density. Fe@C-SN/75 requires greater onset and over potential among its doped variants, this increase in onset potential indicates that there is some optimal doping amount of S, N- at the surface of the catalyst which leads to superior catalytic performance among all, after this further addition of thiourea precursor acts as a retardant in HER activity. Although doped variants of Fe@C require higher cathodic onset potential to ideal zero scale of platinum where $H^+ \leftrightarrow 1/2H_2$ conversion occurs, further variation such as change of doping elements/source and other synthesis parameters is needed to be done to reduce the overpotential. Figure 4.9 (b) shows the corresponding Tafel slopes of all the prepared HER catalysts. Tafel slope is a quantitative measure to evaluate an electrocatalyst and predicts the pathway of H^+ reduction. Fe@C-SN/50 requires 123 mV of overpotential for every ten-fold increase in reaction rate, while for Fe@C-SN/25, we get a lesser slope value of 94 mV dec^{-1}. This value of the Tafel slope shows that HER reaction proceeds through the Volmer reaction, i.e., discharge reaction. [62] Tafel slope value of Fe@C lies far ahead of all three doped samples indicating torpid reaction rate over surface of iron-carbide core and carbon matrix (also *see* Appendix A Table A.4).

Electrochemically active surface area (ECASA) is an important parameter to gauge the actual surface area of the catalyst which is catalytically active. ECASA is calculated by dividing the double-layer capacitance (C_{dl}) with average specific capacitance (C_s) as follow

$$ECASA = \frac{C_{dl}}{C_s} * S \quad \text{.....(Eq. 4.2)}$$

Here, 'S' stands for the geometric area of the electrode. For 'C_{dl}' calculation, CVs of doped samples were performed at scan rates of 20 to 220 mV sec^{-1} in the potential range of 0.1 to 0.2 volt (vs RHE). A comparison CVs of all three doped samples are shown in Figure 4.9 (d) at scan rate of 100 mV sec^{-1}. The plot of current density difference ($\Delta J_{0.15} = J_a - J_c$) *vs* scan rate was plotted as shown in Figure 4.9 (c) and C_{dl} was calculated as half of the linear slope. The C_{dl} values of Fe@C-SN/25 and Fe@C-SN/50 are close to each other and greater to Fe@C-SN/75 showing capacitive properties of the carbon part. The obtained values of ECASA, along with Roughness factor (RF) and specific current density (J_s) at 0.45 V overpotential (η) of all electrocatalysts are tabulated in Table 4.2 (The roughness factor (RF) was calculated by dividing the estimated ECASA by the geometric area of the electrode. The specific current density (J_s) is calculated by dividing the current density per geometric area at a given overpotential (J_g) by the roughness factor (RF) of the surfaces. We used an overpotential value of 0.45 Volt for J_s calculation. Average C_s value is 22 $\mu F/cm^2$)

Table 4.2 ECASA, Roughness factor (RF) and specific current density (J_s) at 0.45 V overpotential (η) of all electrocatalysts.

	ECASA/cm^2	**RF**	**$J_{s,\eta=0.45}$ (mA cm^{-2})**
Fe@C	24.92	356.0	-
Fe@C-SN/25	2.86	40.86	0.0021
Fe@C-SN/50	2.77	39.57	0.0050
Fe@C-SN/75	2.21	31.57	0.0014

The stability of the LSV polarization curve of the catalysts is a critical part of proving its veracity as an electrocatalyst. Figure 4.9 (e) and (f) show polarization curves for Fe@C-SN/25 and Fe@C-SN/50 respectively after 300 and 500 sweeps of CV, an increase in current density output was observed in both samples that can be credited to greater electrode-electrolyte interaction after each CV sweep. Figure 4.10 shows the polarization curves of Fe@C-SN/25 and Fe@C-SN/50 at various scan rates, where a significant increase in current density can be observed which is attributed to enhancement in porosity with each run, hence greater exposures of active sites for H^+ adsorption. LSVs of Fe@C-SN/50 exhibit some irregularity during initial scans; afterward, it follows the increasing pattern. SEM images were collected of all the doped species and undoped Fe@C after multiple sweeps of CV cycles to study any change in morphology under applied charge field and acidic media. No significant change or deterioration of the sample was observed except enhancement in porosity.

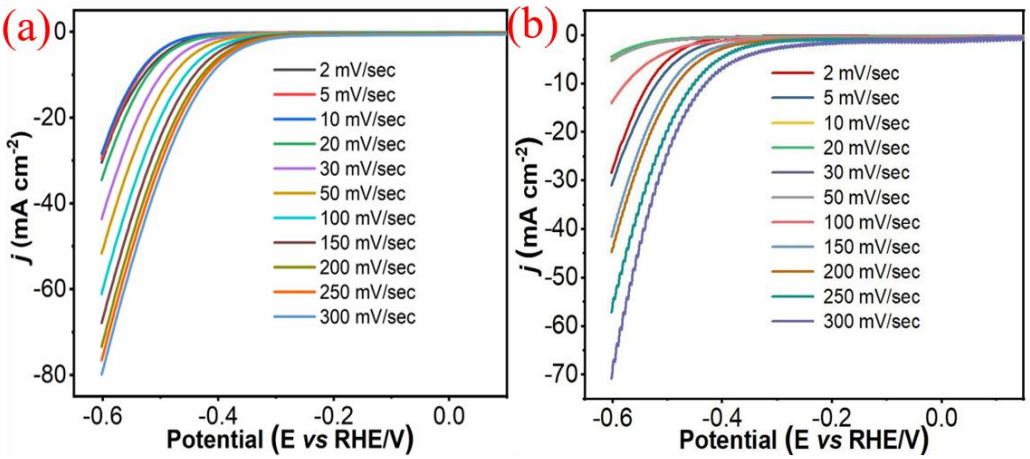

Fig. 4.10 LSV polarization curves of (a) Fe@C-SN/25 and (b) Fe@C-SN/50 at various scan rates.

Earlier reports of iron/iron carbide encapsulated in carbon shell have adopted a complex synthesis approach, while fewer reports are available on the HER performance of such kinds of materials. Our prepared material is different in terms of synthesis strategy and co-doping of two elements N and S into the graphitic encapsulation and matrix using cheap precursor thiourea. One step pyrolytic route yield both doped and un-doped species using the same synthesis strategy. The doped nitrogen has become an integral part of carbon encapsulation and carbon matrix as pyridinic, amino, pyrrolic, graphitic and oxidized N form. The greater pyridinic content in Fe@C-SN/25 and the lower pyrrolic content in Fe@C-SN/50 as compared to others help in greater activity since catalytic activity for N species follows Pyridinic ≈ amino > pyrrolic > graphitic order. [179] Sulphur doping is in the form of thiophene, oxidized S and other associations to carbon. The amalgamation of N and S into carbon structure provides a greater number of active sites with an increase in the graphitic phase of carbon; hence improvement in catalytic activity was observed as compared to un-doped species Fe@C. In terms of catalytic performance, the over-potential required to achieve the current density of 10 mA cm^{-2} is large in comparison to still best suited commercially available 20% Pt/C, but onset potential, Tafel slope and durability of catalyst should also be kept in mind while comparing different catalysts.

4.4 Conclusions

S, N co-doped graphitic carbon encapsulated iron-iron carbide (Fe/Fe_3C) nanostructures were prepared through a one-step pyrolytic route using ferrocene, thiourea and toluene. The crystallographic phases consist predominantly of Fe_3C, metallic Fe and graphitic carbon within the amorphous carbon matrix. Electron

micrographs revealed agglomerated globular-type morphology along with a few tubular structures. Doping precursor thiourea increased not only the number of active sites but also the graphitic phase of carbon shells. The HER performance of the samples in acidic medium didn't follow a monotonic increase with doping; rather, optimum and moderate doping enhances the catalytic activity significantly. Moderately doped samples, i.e., Fe@C-SN/25 and Fe@C-SN/50 both turn out to be catalytically equal in terms of current density output and ECASA value. The Tafel slope of all the doped species is comparatively close to each other. It was observed that the current density of Fe@C-SN/50 increases by ~6.5 fold in comparison to undoped Fe@C species. This sharp increase of current output signified greater H^+ reduction over easily accessible active sites of S and N. Our study highlights the role of optimum S, N-doping in enhancing the catalytic HER performance of iron carbide.